ISSN:2790-1688 Volume-15-(2025)

Motion Simulation and Topology Optimization Design of a Mechanical Gripper Based on Creo Simulate 4.0

Jianyuan Fang

School of International Exchange, Xiangtan University, Xiangtan, China.

932770280@qq.com

Abstract. To optimize the design of the gear mechanical gripper, this study begins with the creation of a schematic diagram of the mechanism using CAD software. The mechanical gripper was modeled in 3D and structurally designed using Creo Parametric 4.0, with relevant data imported into Creo Simulate 4.0 for static strength and stability analysis based on actual load conditions. The analysis identifies the maximum stress occurring at the point of section change in the mechanical gripper. By adjusting the parameters and materials of the gripper, the most optimal design was achieved. Finally, design optimization was performed, resulting in the optimal design of the mechanical gripper. The findings indicate that the stress on the part is below the yield strength of the material, demonstrating reliability and validating the rationality of both the design and material choices.

Keywords: Mechanical Gripper; Automotive Manufacturing; Creo Simulate 4.0; Finite Element Simulation; Topology Optimization Design.

1. Introduction

In the automotive manufacturing industry, the general-purpose two-finger gear-driven mechanical gripper is widely used in various automotive processing scenarios due to its compact structure, precise transmission, and low cost. For instance, it is commonly applied in bar stock gripping processes in automotive chassis mold production plants.

However, frequent gripping failures are often encountered in real-world industrial processing scenarios (Jin et al., 2023). The majority of these failures are caused by structural defects in the mechanical gripper or material failure. Such issues present challenges to the efficiency and safety of automotive manufacturing. In practical applications, the automotive manufacturing industry imposes several requirements on mechanical grippers, including achieving lightweight designs to reduce energy consumption. Furthermore, there are demands to enhance structural strength to adapt to complex working conditions and to control gripping force to ensure the stable transport of workpieces.

To address these challenges, this study focuses on the mechanical gripper used for bar stock gripping in automotive factories, employing finite element analysis software, Creo Simulate 4.0, to perform motion simulation and topology optimization design. First, through static analysis and motion simulation, the study assessed the stress distribution on the mechanical gripper during the bar stock gripping process, identifying design flaws within the structure. Then, to achieve a lightweight design, topology optimization was applied to compare the simulation results of different models, ensuring that structural strength is preserved while enhancing the gripper's performance in automotive manufacturing. Moreover, the reliability and cost-effectiveness of the design have also been improved, reducing production interruptions or failures due to inadequate gripper performance and increasing overall production efficiency, thereby meeting the automotive industry's demands for efficient and stable production.

Both domestic and international research demonstrates significant progress in China's two-finger mechanical gripper technology (Zhang, 2024). However, certain design limitations persist. Wang et al. (2025) developed a digital twin pneumatic robotic hand system, which integrates pneumatic control and flexible gripper mechanisms, allowing for the handling of fragile objects. Despite its advantages, the use of a softer gripper material results in relatively low load-bearing capacity and weak gripping strength. Jing (2013) designed an automatic loading and unloading mechanical gripper for an arc-tooth bevel gear milling machine. This pneumatic-controlled two-finger gripper provides

rapid response and high efficiency. However, the pneumatic transmission system occupies significant space, has a less compact structure, and offers limited load-bearing capacity. Zhang et al. (2024) optimized the structure of a coal gangue sorting mechanical gripper, employing cylinder-controlled opening and closing of the gripper to handle heavy objects. However, the large volume of the gripper, along with the material choice, leads to increased mass, which reduces precision and fails to meet lightweight design objectives. Li et al. (2023) designed a selection mechanical gripper with a three-finger configuration to enhance gripping stability. However, its large size makes it unsuitable for use in confined spaces.

In comparison with other types of mechanical grippers, the gear-driven two-finger gripper selected in this study offers a favorable balance between structural complexity, cost efficiency, functional adaptability, and precision. Its technical advantages make it a preferred solution for industrial material handling, assembly tasks, and similar applications, demonstrating considerable potential for future use. Therefore, this study conducts a detailed design analysis of the gear-driven two-finger mechanical gripper, utilizing Creo 4.0 for three-dimensional modeling and structural design. Static analysis was performed initially, followed by gear load analysis, load calculations (Sheng et al., 2025), and verification of root bending fatigue strength (Yang et al., 2020). The relevant data was subsequently imported into Creo Simulate 4.0 simulation software for static strength and stability analysis, based on actual loading conditions. Appropriate materials and designs were selected, and the rationality of the mechanical gripper's structural design was validated. The design meets the requirements of real-world motion planning (Wang, 2021), while effectively leveraging the material properties (Feng et al., 2020).

2. Structural Design

2.1 3D Modeling Using Creo Parametric 4.0

In accordance with mechanical principles and relevant mechanical design theories, a straight-tooth cylindrical gear drive was employed. The mechanical gripper was modeled in three dimensions using Creo Parametric 4.0, as illustrated in Figure 1.

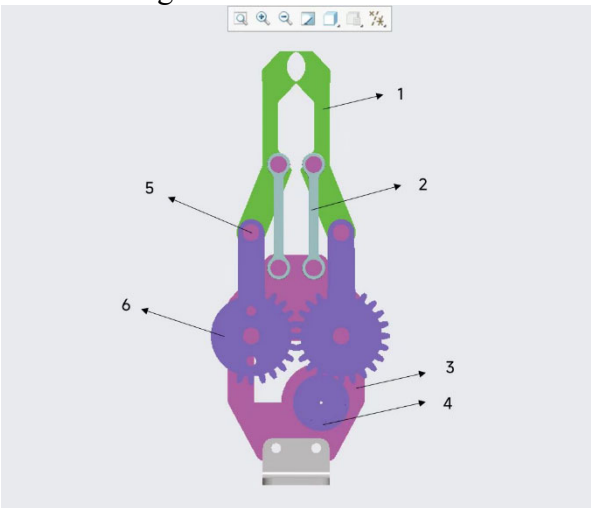

Figure 1. 3D Model of the Gear-Driven Mechanical Gripper

Figure 1 illustrates the gear-driven two-finger mechanical gripper, which is composed of six components. These components are labeled in a clockwise direction as 1, 2, 3, 4, 5, and 6.

The gripper (part 1 in Figure 1) serves as the component that directly contacts the object being grasped, responsible for applying the clamping force to secure or release the object. Its working surface was designed to conform to the shape of the object, enhancing friction and preventing slippage. The linkage (part 2 in Figure 1) functions to transmit motion and mechanical forces. After being hinged with a pin shaft, the linkage converts the rotational motion of the gear arm into a parallel opening and closing motion of the gripper, effectively transferring forces. For instance, it transmits

the driving force (torque) generated by the gear arm to the gripper, thereby enabling the clamping action. Additionally, the linkage plays a crucial role in maintaining the stability of the entire process. The base plate (part 3 in Figure 1), acting as the foundation of the mechanical claw, functions similarly to a frame. Its primary functions include providing support, as the base plate serves as the fixed reference component for the mechanical claw, supporting the installation of all other parts (input gear, fixed gear/gear shaft, gear arm, pin shaft, linkage); and fixation, with threaded holes that allow the entire mechanical claw to be secured to the end of the robotic arm or other devices using screws. The input gear (part 4 in Figure 1) serves as the power input point for the mechanical claw, directly connected to the drive source (the motor's output shaft). When the motor rotates, the driving input causes the gear to rotate. The rotational motion of the input gear provides the primary force that drives the entire clamping action. The gear arm (part 5 in Figure 1) serves as the core component for transmission and motion conversion. It is a composite structure consisting of a gear and an extending arm. The gear arm is mounted on the base plate via a pin shaft, with the gear on it meshing with the input gear. Due to the constrained rotation center of the gear arm, it rotates under the drive of the input gear. The pin shaft (part 6 in Figure 1) is fixed onto the base plate through pressing, serving as the center of rotation for both the gripper and gear, allowing the connected components to rotate around it. It also functions to connect components, such as the gear arm to the base plate, and the linkage to the gripper. The pin shaft also bears shear forces, as it must withstand the shear forces transmitted between the different components.

2.2 Selection of Mechanical Claw Dimensions

The cylindrical workpiece used in this design has a diameter of 10.2 cm and a thickness of 2 cm.

It was assumed that the pitch circle diameter of the gear is 12.18 cm, the pitch circle diameter of the gear arm gear is 25.32 cm, the arm length is 18.34 cm, the linkage length is 31 cm, the front end length of the gripper is 34 cm, the front end width is 4.66 cm, the rear end length is 22 cm, the rear end width is 8.7 cm, the angle between the front and rear ends is 124° , and the thickness is 3 cm. This design is intended for lightweight gripping, with a load capacity ranging from 0.2 to 5 kg, and a dynamic load approximately 60% of the static load value. The accuracy threshold for repeatable positioning was set between ±0.01 mm and ±0.03 mm.

From the sensitivity analysis of the relevant parameters, it was observed that the front end width d and the front end length L of the gripper have a pronounced effect on stress and deformation. Therefore, these two parameters were prioritized as the optimization objectives, with the remaining parameters to be optimized subsequently. The output parameter was set as the magnitude of the stress. The response of the input parameters was defined as the relationship between the input parameters and the output parameter. As a result, a large number of samples were not required, which was assumed as a sample size of 10 in this study. The range of parameter variation is ±10% of the original values. The specific parameters are listed in the table below:

Table 1 Specific parameters of the clamping jaw design point values

Sample Number	Front Width (d) (cm)	Front Length (L) (cm)
1	4.66cm	34cm
2	4.66cm	37.4cm
3	4.66cm	40.8cm
4	4.66cm	44.2cm
5	4.66cm	47.6cm
6	4.66cm	51cm
7	4.25cm	34cm
8	3.83cm	34cm
9	3.42cm	34cm
10	3cm	34cm

Subsequent analysis and optimization of the target samples have been performed using methods such as finite element analysis, ultimately leading to the optimal design of the mechanical claw.

2.3 Schematic Diagram of the Mechanical Claw Mechanism

The mechanical claw structure is fundamentally symmetrical, with each side comprising a planar linkage mechanism and a cylindrical gear mechanism. Low pairs are employed in place of high pairs. Upon decomposition, it is determined that the mechanism consists of one driving member and two second-class lever groups, classifying it as a second-class mechanism. Analysis indicates that the four-bar linkage functions as a double-rocker mechanism, exhibiting neither sudden return behavior nor extreme position angles.

Accordingly, the schematic diagram of the mechanism was drafted using AutoCAD, as shown below:

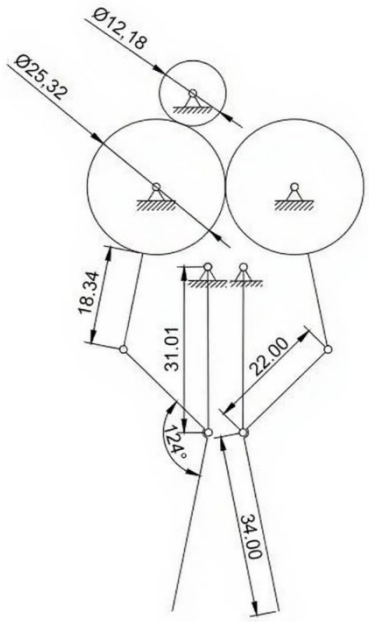

Figure 2. Schematic Diagram of the Mechanical Gripper Mechanism

Each side of the mechanical claw consists of four components, with the kinematic pairs comprising one higher pair and five lower pairs. The degree of freedom is calculated as follows:

$$F=3*n-(2*PL+PH)=3*4-(2*5+1)=1 \quad (1)$$

Consequently, the mechanical claw has a degree of freedom of 1, requiring the integration of one driving component. The mechanism follows a predetermined motion trajectory. In this design, a small gear serves as the input to control the opening and closing of the mechanical claw.

3. Combined Analysis

3.1 Static Analysis

Assuming that both the mechanical claw and the workpiece are composed of 40 steel, the material properties are provided in the table below.

Table 2. Material Properties of FE40

Material	Density (kg·m^{-3})	Poisson's Ratio	Elastic Modulus (GPa)	Yield Strength (MPa)
FE40	7191.21	0.25	126	335

The diameter of the workpiece is 10.2 cm, the height is 2.5 cm, and its volume is $V=\pi r^2h=817.13cm^3=8.17*10^{-4}m^3$.

The mass of the workpiece is $m=\rho V=5.87kg$ (2)

The coefficient of friction between steel and steel is known to be $\mu = 0.15$

Based on this, a force analysis of the workpiece was performed, where the frictional force exerted by the gripper is equal to the gravitational force of the workpiece，$F_f=G$

i.e., $$\mu F = mg \tag{3}$$

It follows that: $F_N=383.89N$

The corresponding force diagram for the gripper is shown below:

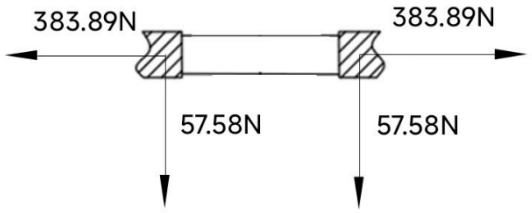

Figure 3. Force Diagram of the Gripper Jaw

3.2 Dynamic Analysis

Initially, an analysis of the gear section was conducted, where the pitch circle diameters of the large and small gears are given as 25.32 cm and 12.18 cm, respectively. The robotic arm gear is required to both transmit power and bear load. To accommodate the load, this study selected the standard modulus from the second series, with a modulus of m=7，$h_a^*=1$，$c^*=0.25$. Through the following calculations:

$$\begin{cases} d=mz \\ h_{a_1}=h_{a_2}=h_a^*m \\ h_{f_1}=h_{f_2}=(h_a^*+c^*)m \\ d_b=d\cos\alpha \\ p=\pi m \\ d_a=(z_1+2h_a^*)m \\ d_f=(z-2h_a^*-2c^*)m \\ e=\pi m/2 \\ a=m(z_1+z_2)/2 \\ i_{12}=d_2/d_1 \end{cases} \tag{4}$$

the gear parameters were derived, as presented in the table below:

Table 3. Gear Parameter Design

Name	Calculation Result
Pressure Angle (α)	20°
Number of Teeth on Small Gear (z_1)	17
Number of Teeth on Large Gear (z_2)	36
Addendum (h_a)	7mm
Dedendum (h_f)	8.75mm
Pitch (p)	22mm
Base Circle Diameter of Small Gear (d_{b1})	114.45mm
Base Circle Diameter of Large Gear (d_{b2})	237.93mm
Addendum Circle Diameter of Small Gear (d_{a1})	133mm
Addendum Circle Diameter of Large Gear (d_{a2})	266mm
Dedendum Circle Diameter of Small Gear (d_{f1})	101.5mm
Dedendum Circle Diameter of Large Gear (d_{f2})	234.5mm

Tooth Space Width (e)	11mm
Standard Center Distance (a)	187.5mm
Transmission Ratio (i_{12})	2.12

Subsequently, the input of the four-bar mechanism was analyzed. It was determined that the rotational speed of the small gear is n1=60r/min, the angular velocity is $\omega = 2\pi$ rad/s, and the input power is P=1kW. From this, the calculation yield:

$$T1=9550*P1/n1=159.17N\cdot m \tag{5}$$

Following the velocity analysis, the velocity relationship of the four-bar mechanism was derived, with the corresponding velocity diagram shown below:

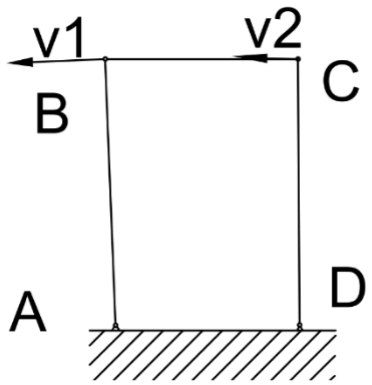

Figure 4. Component Velocity Analysis Diagram

The BC component was selected as the object of study, where V1 represents the absolute velocity, V2 represents the connected velocity, and V_{BC} represents the relative velocity. Since the absolute velocity is the vector sum of the relative velocity and the connected velocity, it gains:

$$V1=V2+VBC \tag{6}$$

From $v=\omega*l$, it was determined that the magnitude of V1 is 1.95 m/s, with its direction perpendicular to rod AB, directed horizontally to the left. The magnitude of V2 was unknown, but its direction was known, being perpendicular to the line CD connecting the rotational center of the connecting rod to point C and pointing to the left. V_{BC} represents the relative velocity, with its magnitude also unknown, and its direction perpendicular to the BC rod.

After calculation, $V2=V1\cos\theta=1.94m/s$, $V_{BC}=V1\sin\theta=0.07m/s$ was obtained.

Next, a strength analysis of the gears was conducted. Due to the applied load, the meshing gears experience bending stress on the gear teeth, which may result in deformation or fracture. This is the primary mode of gear tooth failure. The fundamental formula for calculating the gear load is as follows:

$$\begin{cases} F_{ca}=KF_n \\ \phi_d=\frac{b}{dm_1} \\ K=K_AK_vK_\alpha K_\beta \\ F_n=F_{t1}/\cos\alpha \\ F_{r1}=F_{t1}\tan\alpha \\ F_{t1}=\frac{2T1}{d1} \end{cases} \tag{7}$$

In the formula, K represents the correction coefficient, K_A denotes the usage coefficient, K_v is the dynamic load coefficient, K_β is the tooth load distribution coefficient, K_α is the inter-tooth load distribution coefficient, F_n refers to the normal force acting on the gear, $F_{r1}$is the radial force and F_{t1} represents the normal force.

By substituting K_A=1.25, K_α=1.1, K_β=1.1, K_v=1, the results are K=1.51, F_N=2613.63N, F_{ca}=3946.58N.

Finally, a check was performed on the bending fatigue strength at the root of the gear:

$$\begin{cases} \sigma_F = \dfrac{2K_F T_1 Y_{Fa} Y_{Sa} Y_\varepsilon}{\phi_d m^3 z_1^2} \\ Y_\varepsilon = 0.25 + \dfrac{0.75}{\varepsilon_\alpha} \\ \sigma_{F0} = \dfrac{M}{W} = \dfrac{6F_n cos\text{th}}{bs^2} \end{cases} \tag{8}$$

In the formula, Y_ε represents the fatigue calculation overlap coefficient, W denotes the bending section modulus and Y_{Fa} is the tooth profile coefficient.

Upon verification, $\sigma_F \leq [\sigma_F]$ =125Mpa indicates that the gear system design is feasible.

4. Simulation Analysis

The pressure applied by the gripper is F_N=383.89N, with the contact area on the gripper surface being 35.61 cm^2 , so the load magnitude is 0.11 MPa. The 3D model was imported into Creo Simulate 4.0 and generated the mesh as shown in the figure below, creating a total of 142 elements and 83 nodes.

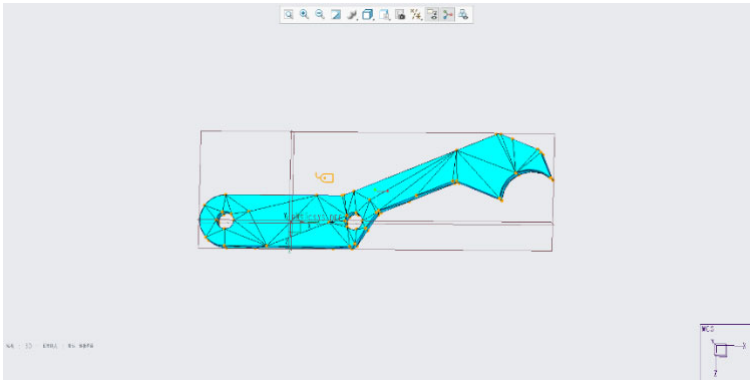

Figure 5. Finite Element Mesh Generation

The pressure load was set to 0.11 MPa, and the gripper was constrained using a pin constraint, which restricts movement along the axial direction while allowing free rotation. The material was defined as FE40. A new static analysis was conducted, and after running the simulation, the following stress results are obtained:

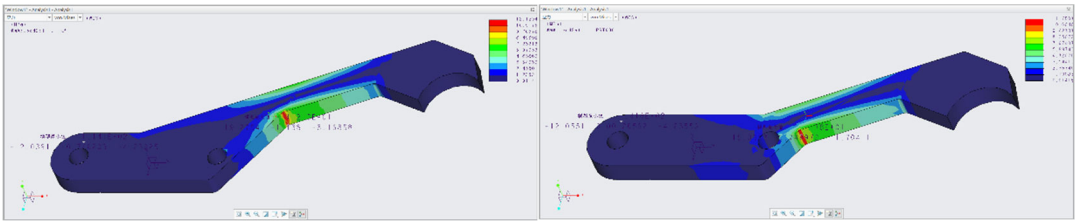

(a) Normal Gripper Stress Distribution (b) Finest Gripper Stress Distribution

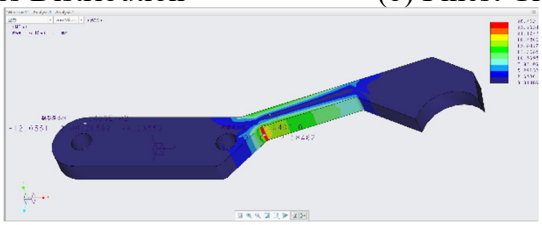

(c) Longest Gripper Stress Distribution

Figure 6. Finite Element Stress Analysis Results

The maximum stress was concentrated at the section where there was a sudden change in geometry. The maximum stress experienced by the standard gripper (with a front width of d = 4.66 cm and a front length of L = 34 cm) was minimal, with a magnitude of 11.78 MPa.

Subsequently, an analysis of the deformation was conducted, with the maximum deformation occurring at the force application area on the front end of the gripper. The results obtained are summarized in the table below:

Table 4. Gripper Analysis Results

Type	Maximum Stress	Maximum Deformation	Mass
Normal Gripper (Sample 1)	11.78Mpa	$9.849*10^{-3}$mm	8.785kg
Longest Gripper (Sample 6)	12.13Mpa	$10.618*10^{-3}$mm	10.643kg
Finest Gripper (Sample 10)	26.40Mpa	$3.666*10^{-2}$mm	8.405kg

Finally, based on the results of the previous static analysis, this study conducted a stability analysis to assess its stability, examine its mechanical performance, and evaluate its ability to resist instability or overturning. The verification results reveal that the maximum stress is concentrated at the section where there is a sudden change in geometry at the front end of the gripper. The maximum stress value is 79.11 MPa, which is significantly lower than the allowable stress limit. This confirms the rationality of both the material selection and the structural strength design.

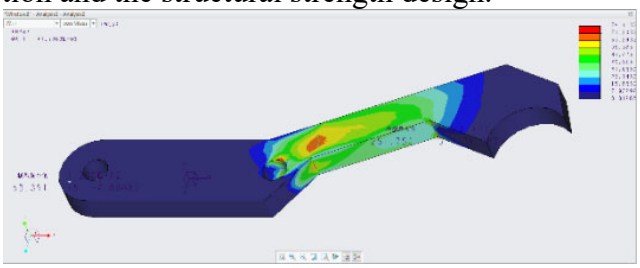

Figure 7. Stability Analysis Results

The results indicate that, through finite element analysis and topology optimization, the design of the gripper using the standard claw reduces the mass by 17.45% compared to the longest claw gripper. The maximum stress and maximum deformation are 11.78 MPa and 9.849×10^{-3} mm, respectively. These values represent the optimal results among the 10 samples and are well below the allowable stress value for the FE40 material. Stability analysis further validates the soundness of the mechanical claw structure design, ensuring that it meets the requirements of practical motion planning while effectively utilizing the material's properties.

5. Conclusion

This paper employs a new design process that integrates three steps: 3D modeling, multi-field analysis, and parameter optimization. Besides, it innovatively combines Creo Parametric 4.0 modeling with Creo Simulate 4.0 simulation. Initially, this study analyzed 10 sets of parameter samples ($\pm$10% fluctuation), which identifies the key influencing factors as the gripper's front width (d) and length (L). Subsequently, deformation and stress analysis was performed on these parameters, optimizing the design parameters. Furthermore, static, dynamic, and finite element analysis methods were integrated, overcoming the limitations of relying on a single analytical approach. The final results validate the reliability of the mechanical claw structure, thereby confirming the rationality of using multiple analytical methods. In the optimization design, this study focuses on balancing structural performance with weight reduction. Simulation was used to identify the location of maximum stress concentration (the section with a sudden geometry change), and this formed the basis for optimizing the gripper's design dimensions. The optimal design was found to be a gripper with a front width of 4.66 cm and a length of 34 cm. Subsequent verification showed that its maximum stress is 11.78 MPa (only 3.5% of the material's yield limit), and the maximum deformation is 9.849×10^{-3} mm, which is well below the safety threshold, confirming the design's reasonableness. Compared to the longest claw, i.e., the gripper designed in Sample 6, the weight was reduced by 17.45%, achieving an optimal balance between weight and strength. Additionally, this study fine-tuned the gear parameters (module = 7, transmission ratio = 2.12) to ensure both transmission

accuracy and compactness of the structure. Ultimately, this enabled the mechanical claw to ensure both reliability and cost-effectiveness during grasping operations.

References

[1] Jin, L., Zhang, Y., Huang, L., et al. (2023). Analysis and troubleshooting of common faults in the automatic sampling and storage system of raw materials in steel enterprises. Today's Manufacturing and Upgrading, 10, 118-120.

[2] Zhang, D. (2024). Simulation analysis of dual-motor driven two-finger mechanical claw based on SOLIDWORKS Simulation. In Proceedings of the Fourth International Conference on Mechanical, Electronics, and Electrical and Automation Control (METMS 2024) (Vol. 13163, pp. 2000-2005). SPIE.

[3] Wang, X., Zhang, M., & Li, B. (2025). Design of a pneumatic manipulator system based on digital twins. Hydraulics and Pneumatics, 49(4), 11-21.

[4] Jing, J. (2013). Design and performance analysis of the automatic loading and unloading mechanical claw for arc-tooth bevel gear milling machine (Master's thesis, Henan University of Science and Technology).

[5] Zhang, B., Wang, H., Dong, Y., et al. (2024). Structural optimization design and finite element analysis of a mechanical claw for coal-gangue sorting. Machine Tool & Hydraulics, 52(1), 183-189.

[6] Li, M., Huang, C., & Wang, T. (2023). Dynamics analysis of a selection claw based on ANSYS. Coal Mine Machinery, 44(4), 90-92.

[7] Sheng, J., Wu, S., Liu, G., et al. (2025). Design and finite element analysis of a dual-motor driven unmanned aerial vehicle mechanical claw. Journal of Nanchang Engineering College, 44(01), 54-61+68.

[8] Yang, K., Cheng, G., Li, Z., & Qian, R. (2020). Fundamentals of Mechanical Design (7th ed.). Beijing: Higher Education Press.

[9] Wang, S. (2021). Transient dynamic analysis of a selection manipulator based on ANSYS. Coal Technology, 40(11), 199-201.

[10] Feng, C., Jiang, K., Wang, Y., et al. (2020). Multi-objective optimization of the reducer high-speed shaft based on ANSYS analysis. Machine Tool & Hydraulics, 48(20), 139-143.